Effect of bonding time on the microstructure and shear property of Cu/SAC-15Ag/Cu 3D package solder joint fabricated by TLP

Li Yang[1,*] , Yuhang Xu[2], Yaocheng Zhang[3], Kaijian Lu[2], Jian Qiao[2], Yao Yang[2], Feng Xu[3], and Huiming Gao[4]

[1] *School of Mechanical Engineering, Guilin University of Aerospace Technology, Guangxi 541004, People's Republic of China*

[2] *School of Mechanical Engineering, Soochow University, Jiangsu 215021, People's Republic of China*

[3] *School of Automatic Engineering, Changshu Institute of Technology, Jiangsu 215500, People's Republic of China*

[4] *National Dies and Molds Quality Supervision Test Center, Jiangsu 215300, People's Republic of China*

ABSTRACT

In this paper, Cu/SAC-15Ag/Cu 3D package solder joints were prepared by transient liquid phase (TLP) bonding technology. The effects of bonding time on the microstructure and shear property of solder joints were investigated. The results indicated that the microstructure of solder joints is coarsened with increasing bonding time. The intermetallic compounds (IMCs) in the interfacial reaction zone consist of Cu_3Sn and Cu_6Sn_5 phase, and the IMCs in the in situ reaction zone include Ag_3Sn phase, Sn-rich phase, and Ag particles. The thickness of interfacial IMCs layer initially decreases due to the volume contraction caused by the transformation from Cu_6Sn_5 to Cu_3Sn, and then increases as a result of the coarsen of Cu_3Sn. The minimum porosity of the solder joints reaches 0.24% under bonding time of 30 min. The shear strength of solder joints increases first and then declines with the extension of bonding time, and the maximum shear strength of 45.3 MPa is obtained by bonding for 30 min. The shear fracture mechanism of solder joints changes from ductile fracture to ductile–brittle mixed fracture, and then changes to brittle fracture. Cracks nucleate at the voids and propagate quickly with prolonging bonding time, and the cracks could be restrained by the voids.

1 Introduction

The third-generation wide band gap semiconductors, such as SiC and GaN, have become potential substitutes for traditional Si semiconductors due to their excellent performance, especially chemical stability and excellent electrical properties at high temperature [1]. SiC chips can work stably at ambient temperature up to 600 °C [2, 3]. The trend of SiC

Address correspondence to E-mail: linlideyu@126.com

Springer

semiconductor servicing at high temperature poses a great challenge to packaging methods and materials.

In recent years, many researches focus on exploring new 3D packaging technology and reliable lead-free high-temperature resistant solder, among which TLP bonding is considered as one of the most promising bonding methods. In the process of TLP bonding, IMC solder joints can be obtained by diffusion reaction between high melting point substrate (such as Cu, Ag substrate) and low melting point interlayer (such as Sn, In) at low temperature. TLP-bonded joints usually have excellent heat resistance which is dominantly ascribed to the remelting temperature of IMC being much higher than that of the original solder [4].

At present, many high-temperature packaging systems have been proposed, such as Cu-Sn and Ag-Sn systems [5, 6], whose research focuses on the growth behavior of IMC [7–9], the formation and elimination of voids [10, 11], the improvement of ductility of IMC [12], and the reduction of soldering time [13, 14]. Sn-0.3Ag-0.7Cu is a kind of better lead-free solder, which has the advantages of good plasticity, low melting point, high strength, low price, good wettability, and thermal fatigue resistance. M. He [15] et al. studied the growth behavior and reliability of IMC in Sn–Ag–Cu solder joints and found that aging experiment accelerates the growth of IMC, promotes the germination and growth of micro kirkendall voids to form larger voids, which becomes one of the potential risks of reliability. The low silver Sn-0.3Ag-0.7Cu solder is far away from the eutectic point. Due to the high supercooling degree during the solidification process, the first precipitated primary crystal grows into coarser grains at high temperature for long dwell time, which leads to the poor mechanical reliability of the lead-free solder and limits its extensive application. L. Yang [16] et al. added nano-BaTiO$_3$ particles to the low silver Sn–Ag–Cu solder for earlier solidification. During the solidification process of the solder, nanoparticles provide nucleation particles for the nucleation of β-Sn phase, making the matrix structure of the solder uniformly refined, thus improving the mechanical properties of the solder joints. L. Sun [17] et al. studied the microstructure evolution and the mechanical properties of Sn–Ag–Cu solder joints with different Ag content. It is found that the interfacial IMC layer thickness increases significantly, and the morphology of interface layer transforms from scallop type to layer type as Ag content increases. In addition, the mechanical properties increase dramatically as well. It reveals that the microstructure, IMCs, and shear property of solder joints are affected by Ag addition. Ag element is an optional alloying element to improve the microstructure and shear property of Sn–Ag–Cu solder joints. However, there are few researches on the effects of bonding time on the solder joints.

In this paper, SAC-15Ag solder was obtained by adding nano-Ag particles to Sn-0.3Ag-0.7Cu (SAC) solder. In order to obtain superior performance solder joint, the effects of bonding time on the microstructure and shear property of Cu/SAC-15Ag/Cu 3D package solder joints were investigated.

2 Experimental

Pure Cu (99.99%) sheets with the dimensions of 10 mm × 10 mm × 4 mm and 12 mm × 12 mm × 4 mm were chosen as the upper and lower substrate, respectively. The substrates were ground and polished to remove oxide e and oil contamination. Ag particle size was chosen as 1 μm and the size of SAC solder powder was 25–45 μm. The SAC-15Ag solder paste was obtained by adding 15 wt. % Ag nanoparticles and 11 wt. % rosin flux into the Sn-0.3Ag-0.7Cu solder powder and stirred in the crucible for 2 h. The lower Cu substrate was put into the mold, and then the solder paste was coated on the lower Cu substrate evenly with a glass piece. Finally, the upper substrate was placed on the lower substrate to form a sandwiched structure (Fig. 1). The Cu/SAC-15Ag/Cu 3D package solder joints were obtained by bonding the sample of sandwiched structure using TWB-100 wafer bonding machine. The bonding process was carried out under vacuum degree of 1-5 Pa by the machine. The samples were bonded at 260 °C and under 1 MPa for a range of 0–120 min (Fig. 2). The cross-sectional microstructure of solder joints was observed by Zeiss supra 55 scanning electron microscope (SEM) equipped with energy dispersive spectroscopy (EDS) after the joints were etched by 5% nitric acid. The phase composition of the solder was determined by X-ray diffraction (XRD). The thickness of IMC layer was evaluated by Nano Measurer software. The porosity of solder joints was evaluated by Image-Pro Plus software.

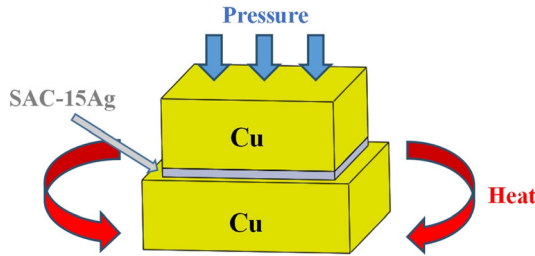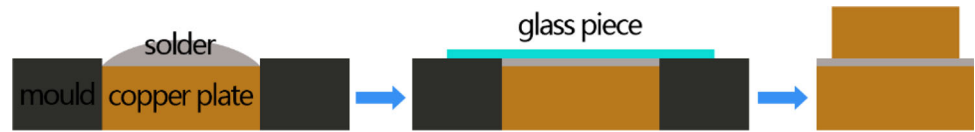**Fig. 1** Schematic diagram of solder coating

**Fig. 2** Bonding process schematic diagram of Cu/SAC-15Ag/Cu 3D package solder joint

The shear test of solder joints was performed by UTM5305 electronic universal testing machine with stretching rate of 0.02 mm/min, and the schematic diagram of shear test is shown in Fig. 3. Shear strength was evaluated by the average of three replicate tests for each joint. The fracture surfaces of solder joints were analyzed by SEM.

3 Results and discussion

3.1 Microstructure

Figure 4 represents the cross-sectional microstructure of the Cu/SAC-15Ag/Cu 3D package solder joints bonded for different times (10 s, 1 min, 10 min, 30 min, 60 min, 120 min). The solder joint includes

Fig. 3 Schematic diagram of shear test
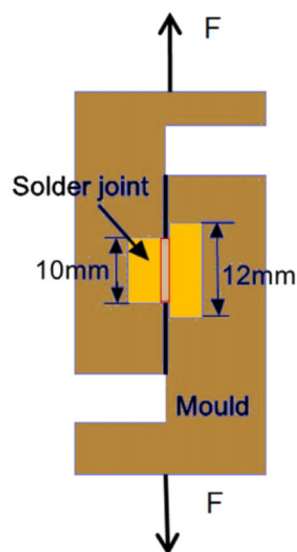
interface reaction zone (I) and in situ reaction zone (II), as shown in Fig. 4a. The solder joint, bonded for 10 s, consists of layer-shaped IMC, scallop-shaped IMC in zone I, and island-shaped IMC in zone II. The island-shaped IMC is surrounded by the dark gray IMC with evenly dispersed white particles. As listed in Table 1, EDS results show that the layer-shaped IMC is Cu_3Sn phase, the scallop-shaped IMC is Cu_6Sn_5 phase, and the island-shaped IMC is Ag_3Sn phase. The dark gray IMC is Sn-rich phase and the white particles are Ag particles. There are few voids in the in situ reaction zone and the porosity of the solder joint is 1.75%. The thickness of Cu_3Sn phase layer increases from 1.63 μm to 5.51 μm, while the thickness of Cu_6Sn_5 phase layer decreases with the increase of bonding time. Cu_6Sn_5 phase is not detected by EDS in the solder joint bonded for 10 min. The morphology of Ag_3Sn phase varies from island shape to flaky shape, and the contents of Sn-rich phase and Ag particles reduce. Sn-rich phase is exhausted with bonding time exceeding 30 min, and cracks nucleate with bonding time over 120 min. The minimum porosity of the solder joints reaches 0.24% when the bonding time is 30 min.

The interfacial IMCs consist of Cu_6Sn_5 and Cu_3Sn. The formation of Cu_6Sn_5 and Cu_3Sn occurs along the solder/Cu substrate layer of solder joints, it can be expressed as Eq. (1) and (2) [18–21]:

$$5Sn + 6Cu \rightarrow Cu_6Sn_5 \tag{1}$$

$$Cu_6Sn_5 + 9Cu \rightarrow 5Cu_3Sn \tag{2}$$

Cu atoms diffuse along the direction perpendicular to the interface between substrate and solder, which is controlled by diffusion driving force. The diffusion driving force is caused by the concentration difference of Cu atoms in the substrate and solder. The scallop-shaped Cu_6Sn_5 phase forms in the interface reaction zone and Cu_3Sn phase occurs at the interface between Cu_6Sn_5 and Cu substrate.

Figure 5 shows the interfacial IMCs layer thickness of the Cu/SAC-15Ag/Cu 3D package solder joints bonded for different times. The interfacial IMCs layer thickness decreases first and then increases with prolonging bonding time. The volume change rate of
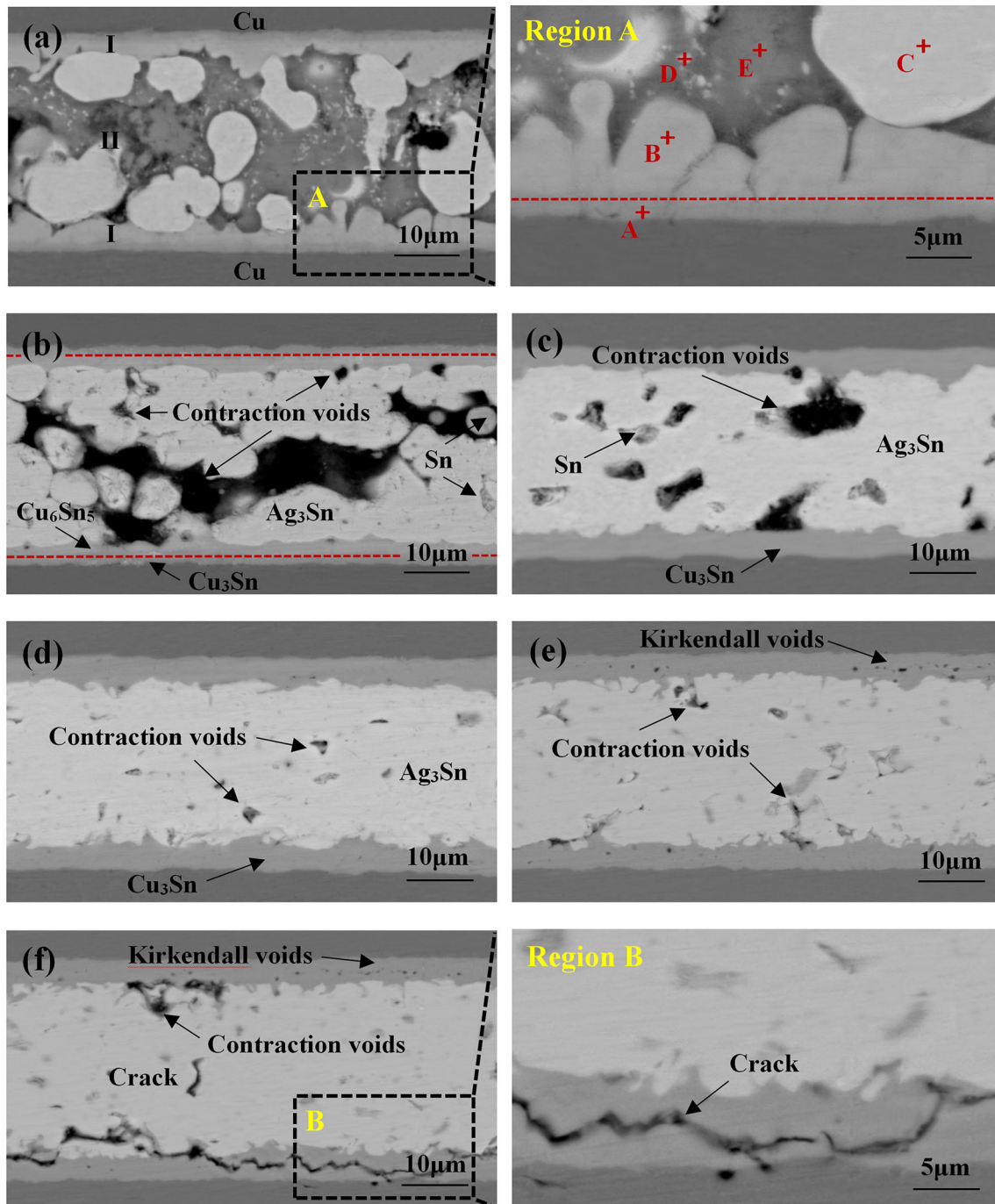
Fig. 4 Cross-sectional microstructure of the Cu/SAC-15Ag/Cu 3D package solder joints bonded for different times: **a** 10 s, **b** 1 min, **c** 10 min, **d** 30 min, **e** 60 min, and **f** 120 min

the transformation from Cu_6Sn_5 to Cu_3Sn phase is computed by Eq. (3) and (4):

$$V = \frac{M}{\rho} \tag{3}$$

$$\Delta V = \left(\frac{(V_{Cu_6Sn_5} + 9V_{Cu}) - 5V_{Cu_3Sn}}{V_{Cu_6Sn_5} + 9V_{Cu}} \right) \times 100\% \tag{4}$$

where V is molar volume, M is molar mass, and ρ is density. ΔV is volume change rate, $V_{Cu_6Sn_5}$, V_{Cu}, and V_{Cu_3Sn} are molar volume of Cu_6Sn_5, Cu, and Cu_3Sn. The physical parameters of Cu_3Sn and Cu_6Sn_5 phase are listed in Table 2 [22]. Based on Eq. (3) and (4), ΔV is computed as 4.38%. The thickness of interfacial

Table 1 EDS results of indicated zone in Fig. 4

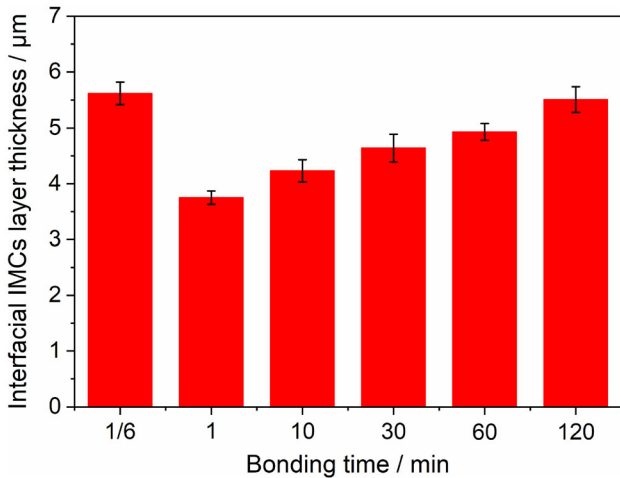| Point	IMCs (at. %)			Phase
	Sn	Ag	Cu	
A	22.25	–	77.75	Cu_3Sn
B	48.04	–	51.96	Cu_6Sn_5
C	26.41	73.59	–	Ag_3Sn
D	5.03	94.45	0.52	Ag
E	97.34	2.23	0.43	Sn-rich

Fig. 5 Interfacial IMCs layer thickness of the Cu/SAC-15Ag/Cu 3D package solder joints bonded for different time

IMCs layer decreases from 5.62 μm to 3.75 μm with increasing bonding time. When the bonding time exceeds 10 min, Cu_6Sn_5 phase is completely transformed into Cu_3Sn phase, and the interfacial IMC layer thickness gradually increases with the increase of bonding time.

In addition, the thermal and electrical properties of Cu_6Sn_5 are inferior to those of Cu_3Sn [23]. The increase of Cu_3Sn phase content is conducive to improve the thermal and electrical properties of solder joints, but sufficient time is needed to convert all

Table 2 Molar mass and density of each phase

Physical parameters	Molar mass (g/mol)	Density (g/cm³)
Sn	118.7	7.28
Cu	64.0	8.93
Cu_6Sn_5	977.5	8.28
Cu_3Sn	310.7	8.90

Cu_6Sn_5 to Cu_3Sn. The XRD results (Fig. 6) of solder joints reveal that the diffraction peaks of Sn and Cu_6Sn_5 phase only appear in the solder joint bonded for 10 s. With bonding time exceeding 30 min, Sn is exhausted and only Cu_3Sn exists in the interface reaction zone, indicating that Cu_6Sn_5 is completely transformed into Cu_3Sn.

Figure 7 represents the porosity of the Cu/SAC-15Ag/Cu 3D package solder joints bonded for different time. The total pixel N of the connection layer and the pixel n of the voids are extracted by Image-Pro Plus software. The porosity of the joint is calculated by the division of n and N. The porosity initially increases, then decreases, and finally increases with prolonging bonding time. The maximum porosity of solder joints reaches 16.35% due to the contraction voids (Cv). Contraction voids are formed as a result of the volume contraction in the Sn-Ag reaction, which are shown in the following equations [24]:

$$3Ag + Sn \rightarrow Ag_3Sn \tag{5}$$

The porosity of solder joints decreases on account of long-term bonding under a constant pressure of 1 MPa when the bonding time is 10 min. However, these voids cannot be eliminated completely by the applied pressure. The minimum porosity of solder joints is 0.24% under bonding time of 30 min. Kirkendall voids (Kv) nucleate after the bonding time exceeds 60 min, which increases the porosity of the solder joint.
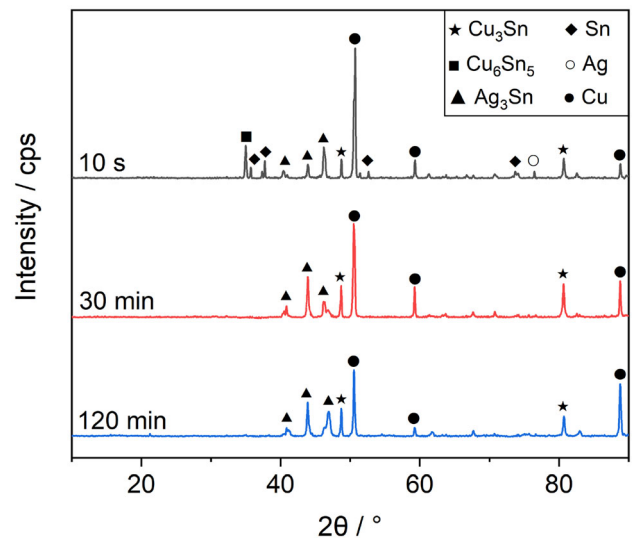

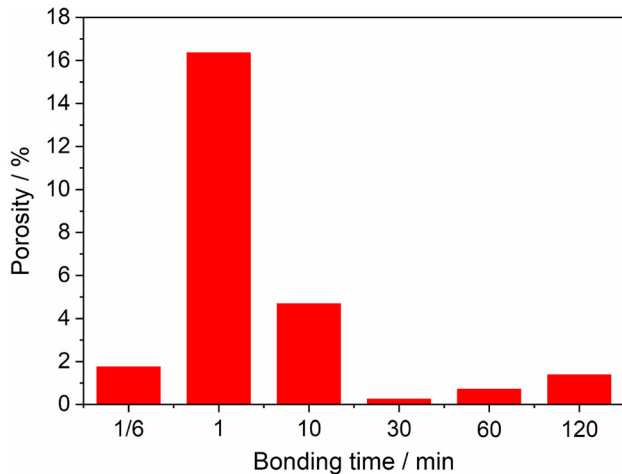**Fig. 6** XRD results of the Cu/SAC-15Ag/Cu 3D package solder joints bonded for different time

Fig. 7 Porosity of the Cu/SAC-15Ag/Cu 3D package solder joints bonded for different time

Fig. 8 Shear strength of the Cu/SAC-15Ag/Cu 3D package solder joints bonded for different times

The formation of kirkendall voids is dominantly produced by the difference on the diffusivity of Cu and Sn atoms, and this unbalanced diffusion mechanism results in the generation of atom level voids with bonding time exceeding 60 min (Fig. 4e-f). In Sn/Cu diffusion couple, the diffusivity ratio of Cu to Sn is approximately 0.35 and 30 in Cu_6Sn_5 and Cu_3Sn [25], respectively. Therefore, Sn is the dominant diffusing component in Cu_6Sn_5, while Cu is the dominant diffusing component in Cu_3Sn. In particular, the formation of Cu_3Sn may produce Kirkendall voids due to the prominent difference on the diffusivity between Cu and Sn atoms in Cu_3Sn [26].

3.2 Shear property

Figure 8 presents the shear strength of the Cu/SAC-15Ag/Cu 3D package solder joints bonded for different time. The shear strength of the joints initially increases and then decreases with prolonging bonding time. The poor shear strength of the joint bonded for 10 s is due to the numerous Sn-rich phases in the in situ reaction zone. The weak interfacial cohesion between solder and substrate is a result of the poor mechanical properties of Sn-rich phase, effecting the shear strength of the solder joint. The maximum shear strength reaches 45.27 MPa of the solder joint bonded for 30 min. The excellent shear property of the joint bonded for 30 min is caused by the precipitation strengthening. The high-temperature solid solution Cu, Sn, and Ag precipitated as Cu_6Sn_5, Cu_3Sn, and Ag_3Sn. Cu_6Sn_5 had completely transformed to Cu_3Sn, of which the mechanical properties
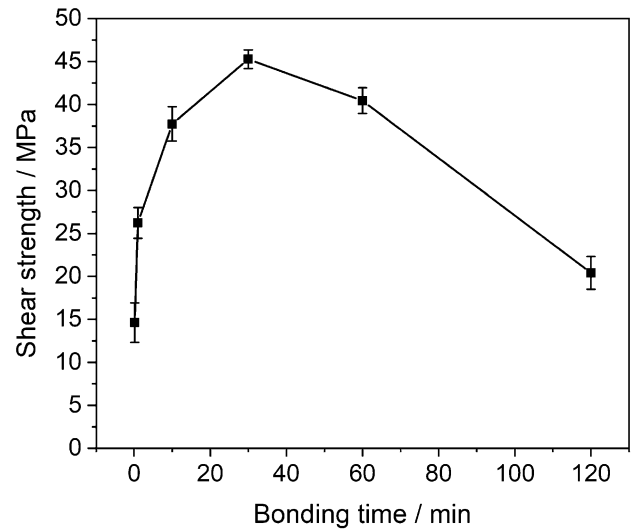
are superior to Cu_6Sn_5 [22]. In addition, the minimum porosity of the solder joint enhances the interconnection between the substrate and the solder matrix, improving the shear property. The volume expansion produced by the thickening of interfacial IMC layer with increasing bonding time causes the shear stress at interface, then promotes crack initiation, resulting in the deterioration of the shear property of the solder joint [27–29]. The heat diffusion of the solder joints is hindered by the formation of voids and cracks with bonding time exceeding 120 min, which promotes the formation of voids and the excessive IMC layer growth conversely, reducing the shear property of the joint.

Figure 9 shows the shear fracture surfaces of the Cu/SAC-15Ag/Cu 3D package solder joints bonded for different times. The dimples are observed on the shear fracture surface of the solder joint bonded for 10 s, showing that the shear fracture mechanism is ductile fracture. Partly river-like structure identified by Cu_3Sn is observed on the shear fracture surface of the solder joint bonded for 10 min, which presents the cleavage surface. Meanwhile, the obvious laceration zone identified by Ag_3Sn appears on the surface, which presents the ductile characteristic, indicating that the fracture mode of the joint is ductile–brittle mixed fracture. The interfacial IMC layer is conducive to show a relatively obvious brittle characteristics after the thickness of IMC layer exceeds a certain critical value, facilitating the fracture [29, 30]. The brittle fracture characters of river-
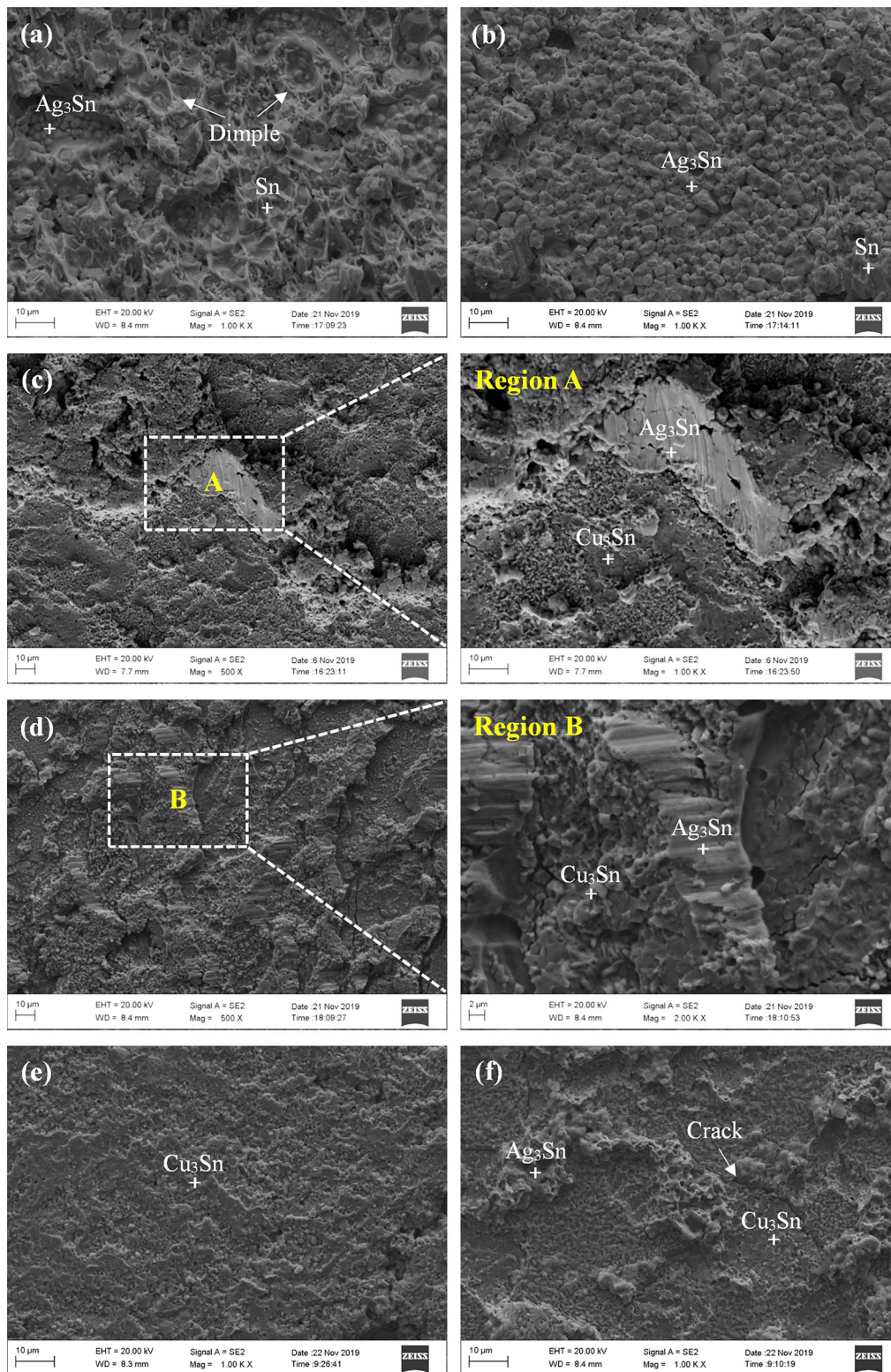
Fig. 9 Shear fracture surfaces of the Cu/SAC-15Ag/Cu 3D package solder joints bonded for different time: **a** 10 s, **b** 1 min, **c** 10 min, **d** 30 min, **e** 60 min, and **f** 120 min
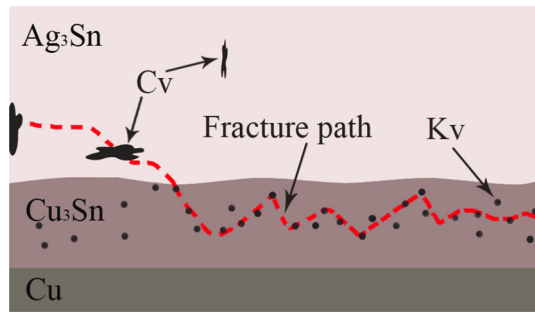
Fig. 10 Illustration of fracture path in the Cu/SAC-15Ag/Cu 3D package solder joint bonded for 120 min

like structure are observed on the shear fracture surface of the solder joint bonded for 60 min, and a small number of cracks are observed on the shear fracture surface of the solder joint bonded for 120 min, as shown in Fig. 9e-f. The shear fracture mechanism of solder joints initially changes from ductile fracture to ductile–brittle mixed fracture, and then changes to brittle fracture with the increase of bonding time. The solder joints bonded for 10 s and 1 min primarily fractured in the in situ reaction zone, while the other joints mainly fractured at the interface between the diffusion reaction zone and the in situ reaction zone.

Figure 10 shows the illustration of fracture path in the Cu/SAC-15Ag/Cu 3D package solder joint bonded for 120 min. Under the shear stress produced by the thickening of interfacial IMC layer and the shear stress produced by shear test, the IMCs between adjacent voids deform greatly, and then the micro-plastic instability occurs. At this time, the void expands rapidly until it shrinks into a line; thus, crack nucleates at the voids and propagates in a zigzag straight line quickly. Finally, because the connection between IMC and IMC is too few, the joint fractures. However, the voids may have an effect on restraining the crack growth. The J-integral (driving force) for the crack without a void in front of it is few times larger than that with a void in the solder joint [31]. This means that the crack could be restrained by the void, and the crack grows along Kv and Cv, as shown in Fig. 10.

4 Conclusions

(1) Bonding time determines the microstructure of solder joints. The thickness of interfacial IMC decreases first and then increases with prolonging bonding time. The interfacial IMC consists of Cu_3Sn phase, and the IMC in the in situ reaction zone is Ag_3Sn phase with bonding time exceeding 30 min.

(2) The porosity of solder joints initially increases, then decreases, and finally increases with the extension of bonding time. The minimum porosity of solder joints is 0.24% with bonding time being 30 min.

(3) The shear strength of the joints increases first and then decreases with the increase of bonding time. The maximum shear strength reaches 45.27 MPa of the solder joint bonded for 30 min. The shear fracture mechanism of solder joints initially changes from ductile fracture to ductile–brittle mixed fracture and then changes to brittle fracture.

(4) Under the shear stress produced by interfacial IMC and shear test, voids expand rapidly until they shrink into a line; thus, cracks nucleate at the voids and propagate, and the cracks could be restrained by the voids.

Compliance with ethical standards

Conflict of interest We declare that we do not have any commercial or associative interest that represents a conflict of interest in connection with the work submitted.

References

1. L.A. Navarro, X. Perpina, P. Godignon, J. Montserrat, V. Banu, M. Vellvehi, X. Jorda, I.E.E.E.T. Power, Electr. **29**, 2261 (2014)
2. W. Zhou, X. Zhong, K. Sheng, I.E.E.E.T. Power, Electr. **29**, 2329 (2014)

3. R. Wang, D. Boroyevich, P. Ning, Z. Wang, F. Wang, P. Mattavelli, K.D.T. Ngo, K. Rajashekara, I.E.E.E.T. Power, Electr. **28**, 555 (2013)

4. J.F. Li, P.A. Agyakwa and C.M, Acta Mater. **59**, 1198 (2011)

5. H. Shao, A. Wu, Y. Bao, Y. Zhao, L. Liu, G. Zou, Ultrason. Sonochem. **37**, 561 (2017)

6. H. Shao, A. Wu, Y. Bao, Y. Zhao, G. Zou, Mat. Sci. Eng. A-Struct. **680**, 221 (2017)

7. H. Shao, A. Wu, Y. Bao, Y. Zhao, G. Zou, T. Nonferr, Metal. Soc. **27**, 722 (2017)

8. H. Liu, K. Wang, K.E. Aasmundtveit, N. Hoivik, J. Electron. Mater. **41**, 2453 (2012)

9. C. Hang, Y. Tian, R. Zhang, D. Yang, J. Mater. Sci-Mater. El. **24**, 3905 (2013)

10. H. Shao, A. Wu, Y. Bao, Y. Zhao, J. Mater. Sci. **52**, 3508 (2017)

11. K. Chu, Y. Sohn, C. Moon, Scripta. Mater. **109**, 113 (2015)

12. N.S. Bosco, F.W. Zok, Acta Mater. **53**, 2019 (2005)

13. X. Liu, S. He, H. Nishikawa, Scripta. Mater. **110**, 101 (2016)

14. B. Liu, Y. Tian, J. Feng, C. Wang, J. Mater. Sci. **52**, 1943 (2017)

15. M. He, F. Wu, W. Zhang, Y. Wu, B. An, Electronic quality. **08**, 25 (2006)

16. L. Yang, J. Ge, Y. Zhang, J. Dai, Y. Jing, J. Mater. Sci-Mater. El. **26**, 613 (2015)

17. L. Sun, M. Chen, L. Zhang, F. Yang, Acta metalica Sinica. **53**, 615 (2017)

18. F. Wang, L. Zhou, X. Wang, P. He, J. Alloy. Compd. **688**, 639 (2016)

19. Q.K. Zhang, Z.F. Zhang, Mater. Sci. Eng. A-Struct. **530**, 452 (2011)

20. F. Li, X. Li, Y. Yan, Fail. Anal. Prev. **1**, 23 (2008)

21. L. Yang, L. Zhu, Y. Zhang, S. Zhou, Y. Xiong, P. Wu, Mater. Res. Express. **5**, 1 (2018)

22. H.P.R. Frederikse, R.J. Fields, A. Feldman, J. Appl. Phys. **72**, 2879 (1992)

23. K.N. Tu, U. Gösele, Appl. Phys. Lett. **86**, 093111 (2005)

24. Y. Bao, A. Wu, H. Shao, J. Mater. Sci-Mater. El **29**, 10246 (2018)

25. A. Paul, C. Ghosh, W.J. Boettinger, Metall. Mater. Trans. A. **42**, 952 (2011)

26. M.J.M. Hermans, M.H. Biglari, *The ELFNET Book on Failure Mechanisms, Testing Methods, and Quality Issues of Lead-Free Solder Interconnects* (Verlag London Limited, Springer, 2011), pp. 105–122

27. H. Sun, Q. Li, Y.C. Chan, J. Mater, Sci-Mater. El. **25**, 4380 (2014)

28. P. Liu, P. Yao, J. Liu, J. Alloy. Compd. **486**, 474 (2009)

29. C. Yu, Y. Yang, K. Wang, J. Xu, J. Chen, H. Lu, J. Mater. Sci-Mater. El. **23**, 124 (2012)

30. H.T. Lee, M.H. Chen, H.M. Jao, T.L. Liao, Mat. Sci. Eng. A-Struct. **358**, 134 (2003)

31. J. Lau, S. Erasmus and S. Pan, in *52nd Electronic Components and Technology Conference* (2002), pp. 992–1000